Received 30 August 2021; accepted 13 September 2021. Date of publication 16 September 2021; date of current version 24 September 2021.

Digital Object Identifier 10.1109/OJCOMS.2021.3113088

Experimental Exploration of Unlicensed Sub-GHz Massive MIMO for Massive INTERNET-OF-THINGS

GILLES CALLEBAUT [1], SARA WILLHAMMAR [1,2] (Member, IEEE), ANDREA P. GUEVARA [1], ANDERS J. JOHANSSON [2] (Member, IEEE), LIESBET VAN DER PERRE [1,2] (Member, IEEE), AND FREDRIK TUFVESSON [2] (Fellow, IEEE)

[1]Department of Electrical Engineering, KU Leuven (Gent Campus), 9000 Gent, Belgium

[2]Department of Electrical and Information Technology, Lund University, 221 00 Lund, Sweden

CORRESPONDING AUTHOR: G. CALLEBAUT (e-mail: gilles.callebaut@kuleuven.be)

This work was supported by the European Union's Horizon 2020 under Grant 732174 (ORCA Project) and Grant 731884 (IoF2020 Program—IoTrailer use case).

ABSTRACT IoT networks are getting overcrowded following the vast increase in number of Internet-of-Things (IoT) devices and connections. Networks can be extended with more gateways, increasing the number of supported devices. However, as investigated in this work, massive MIMO has the potential to increase the number of simultaneous connections and moreover lower the energy expenditure of these devices. We present a study of the channel characteristics of massive MIMO in the narrowband unlicensed sub-GHz band. The goal is to support IoT applications with strict requirements in terms of number of devices, power consumption, and reliability. The assessment is based on experimental measurements using both a uniform linear and a rectangular array. Our study demonstrates and validates the advantages of deploying massive MIMO gateways to serve IoT nodes. While the results are general, here we specifically focus on static nodes. The array gain and channel hardening effect yield opportunities to lower the transmit power of IoT nodes while also increasing reliability. The exploration confirms that exploiting large arrays brings great opportunities to connect a massive number of IoT devices by separating the nodes in the spatial domain. In addition, we give an outlook on how static IoT nodes could be scheduled based on partial channel state information.

INDEX TERMS Channel measurements, low-power wide-area networks, massive MIMO, Internet-of-Things, sub-GHz, test-bed and trials.

I. TOWARDS MASSIVE AND RELIABLE IOT: THE POTENTIAL OF MULTIPLE ANTENNA SYSTEMS

INTERNET-OF-THINGS technology opens up a plethora of new applications and services in various domains. Examples include smart sustainable city services, precision farming, environmental monitoring and efficient utilities. These applications pose requirements on the wireless connectivity beyond what is offered by current networks. In particular, (i) the projected massive number of devices to be supported, (ii) the stringent energy constraints of the IoT nodes, and (iii) the need to establish reliable connections, ask for innovative wireless transmission approaches. Low-Power Wide-Area Networks (LPWANs) operating in unlicensed sub-GHz spectrum are of interest to many IoT applications. They incur no or only a small subscription cost, and the operation at relatively low frequencies offers good coverage [1]. In this paper we study the potential of deploying multiple antenna systems to upgrade these LPWANs to support future IoT services. We focus in particular on massive multiple-input and multiple-output (MIMO) technology as it bears a great potential in view of the above listed requirements:

1) It can support an unprecedented number of simultaneous connections through extensive spatial multiplexing.
2) It typically operates with low complexity single antenna terminals. It allows to considerably reduce the transmit power at the node side thanks to the significant array gain at the base station side.

3) It offers an increased reliability of the links due to the experienced channel hardening effect.

New approaches and technologies need to be adopted to accommodate the massive increase of IoT devices. In [2], the authors use a maximum-likelihood strategy to decode two colliding users based on an interference model. This technique further extends the amount of supported devices in the network. Other work has considered diversity techniques to improve IoT technologies. In [3] Snipe is introduced, which is an IoT system deploying two antennas to coherently combine the received signals at the gateway. Spatial diversity is exploited in [4] by coherently combining weak signals of different gateways in the cloud. The system, Charm, improves the range up to three times and the IoT battery-life fourfold. Including multiple antennas at the gateway is also proposed by [5], where this is theoretically analyzed. However, the authors consider only commercially available hardware and are therefore unable to use maximum ratio combining and are hence rather analyzing a selection combing technique.

The potential benefits of massive MIMO for IoT have been studied in theoretical work such as [6]–[12]. Yet, whether this potential can be realized in real network deployments heavily relies on favorable characteristics of the radio propagation channels [13], [14]. In particular, many studies have assumed independent and identically distributed (i.i.d.) Rayleigh fading channels [5], [7], [12]. Measurement-based studies have shown that the reality deviates from this [15]–[17] and for example significant correlation is often observed over the antennas in the array [16]. Consequently, the channel hardening encountered is less pronounced than predicted by the Rayleigh fading model [15]. Furthermore, different array topologies have been considered as they each favor different environments. For example, in [18] it is demonstrated that an L-structured array outperforms both the uniform linear array (ULA) and the uniform rectangular array (URA) configuration. Hence, they advocate to also consider unconventional array structures.

Previous work has primarily focused on broadband transmission technologies [12], [19]–[22]. As a novel contribution, we study unlicensed narrowband low-power and long-range communication. Unlicensed massive MIMO has been studied in other work in the context of spectrum sharing [23]. However, to the best of our knowledge, no studies have reported on massive MIMO to support LPWANs.

While the results are generally applicable, we here focus on communication tailored for IoT. This means that (i) a narrowband signal is used, (ii) the carrier frequency is sub-GHz, (iii) the number of gateway antennas are more limited than in cellular networks and (iv) the nodes can be considered static. As such, we consider 32 antenna elements and no movement of the devices.

Whereas commonly the single-antenna device is denoted as the user equipment (UE) in a massive MIMO or Long-Term Evolution (LTE) context, in an Internet-of-Things setting the term *node* or *IoT node* is used. As we study the effects of massive MIMO in an Internet-of-Things setting, we use the term node to depict the end-device or single-antenna device.

In this paper, we assess the potential of deploying massive MIMO in the unlicensed sub-GHz band for upgraded IoT connectivity based on the measured channel responses. Thereto, we report on the experimental characterization of narrowband sub-GHz channels with different array configurations. The architecture and implementation of the experimental test set-up is further elaborated on in [24]. More specifically, the antenna design and holders, the limitations of operating in a license-exempt band and how it is implemented is discussed. Furthermore, the experimental campaign is elaborated on and the raw open-source data is referenced. Some first results are shown to evaluate the experiment.

To summarize, our contributions reported on here are (i) an analysis of channel propagation characteristics for large antenna array systems[1] and (ii) an assessment of massive MIMO opportunities and challenges for IoT. We demonstrate – based on the measurements – that the reliability and the number of simultaneous connections can be increased. Furthermore, the array gain can extend the coverage of the base station or allows to reduce the transmit power of the IoT devices. Despite the benefits, some challenges remain such as relatively large antennas and arrays and sporadic traffic that may result in a large overhead, requiring a new set of massive MIMO-specific protocols.

This paper is further organized as follows. In the next section, we introduce the system model and theoretic fundamentals. Section III introduces the measurement setup and scenarios. In Section IV, we present the exploration and assessment performed based on the experiments. Finally, in Section V the main conclusions of this paper are summarized and an outlook on future progress towards massive MIMO-upgraded networks for future IoT is given.

Throughout the paper, vectors are denoted by boldface lower case ($\mathbf{x}$) and matrices by boldface capital letters ($\mathbf{X}$). The superscripts $(\cdot)^{\mathsf{T}}$ and $(\cdot)^{H}$ are used to denote the transpose and the conjugate transpose operations, respectively. The absolute value is denoted by $|\cdot|$, $\|\cdot\|$ denotes the ℓ_2 norm and $\|\cdot\|_F$ is the Frobenius norm or Euclidian norm. The notations $\mathbb{E}\{\cdot\}$ and $\mathbb{V}\{\cdot\}$ denote the expectation and the variance of a random variable, respectively. An overline, e.g., $\bar{\mathbf{x}}$, indicates a normalized quantity. The eigenvalues of a matrix are obtained by the operator $\lambda(\cdot)$. The optional subscripts $(\cdot)_{\min}$ and $(\cdot)_{\max}$ are used to get the minimum and maximum value. The set of complex numbers is denoted by the symbol $\mathbb{C}$.

II. SYSTEM MODEL AND THEORETIC FUNDAMENTALS

Channels: The channels are estimated for each base station (BS) antenna at different node positions and for different

1. The collected data is available at: dramco.be/massive-mimo/measurement-selector/#Sub-GHz.

TABLE 1. Measurement setup.

Parameter	Symbol	Value
Carrier frequency	f_c	869.525 MHz
Number of subcarriers (15 kHz)	F	2
Number of snapshots	N	1000[a]/6000[b]
Transmit power (coerced)	P_{tx}	22.6 dBm
Number of base station antennas	M	32
Number of IoT nodes	K	-
Base station array configuration		ULA/URA
Type of BS antenna		Patch
Type of UE antenna		Dipole
Sample interval		10 ms
Sample duration		66.67 µs
Modulation		OFDM
Subcarrier modulation		QPSK
UE height		1.5 m
BS height		7 m
Antenna polarization		vertical

[a] For static measurements.
[b] For continuous measurements.

frequency points and time instances. An overview of the system parameters and used symbols can be found in Table 1. The total number of antennas is denoted by M. The subscript m specifies the antenna index. The total number of node positions is denoted by K and a given position index by k. As elaborated in [24], the channel is estimated over two frequency points F at different time instances N, with f and n denoting the frequency point and time instance index, respectively. Consequently, a channel matrix for a position k is expressed as $\mathbf{H}_k \in \mathbb{C}^{N\times F\times M}$. Note that the collected channel includes both small-scale and large-scale fading, as well as potential effects from the hardware and interfering devices. As a baseline to compare our results, we use the i.i.d. complex Gaussian channel, i.e., Rayleigh fading channel, as commonly used in theoretical studies. This is modeled as a complex random variable with zero mean and unit variance of power ($h \sim \mathcal{CN}(0, 1)$).

Channel Estimation: The channel is estimated by sending a unique pilot signal from each single-antenna device to the base station. Each device sends a pilot signal at a dedicated frequency, i.e., during the pilot phase all devices use distinct frequencies. The BS can estimate the channel response for each device at a specific location k based on the *a priori* known pilot sequence. The estimated channel is derived by correlating the complex conjugate of the pilot $\boldsymbol{\phi}$ with the received uplink signal $\mathbf{y}$:

$$\hat{\mathbf{h}}_k = \mathbf{y}\boldsymbol{\phi}^H \ . \tag{1}$$

The vector $\hat{\mathbf{h}}_k \sim \mathbb{C}^M$ denotes the estimated channel response between the M antennas and the single-antenna device at position k. For further analysis and readability, we will be using the vector $\mathbf{h}$ to denote the estimated noisy channel $\hat{\mathbf{h}}$.

Normalization: The channel $\mathbf{h}_k(n, f)$ at each position k is normalized such that the average channel gain over all antennas, frequencies and snapshots is equal to one, i.e., $\|\bar{\mathbf{h}}_k\| = 1$, i.e.,

$$\bar{\mathbf{h}}_k(n,f) = \frac{\mathbf{h}_k(n,f)}{\sqrt{\frac{1}{NFM}\sum_{n=1}^{N}\sum_{f=1}^{F}\sum_{m=1}^{M}\left|h_{k,m}(n,f)\right|^2}}. \tag{2}$$

Channel hardening: We assess the channel hardening as a representative characteristics for the decrease of the fading with increasing number of antennas, by which the channel becomes more deterministic and the reliability of the link improves. According to [25], a channel $\bar{\mathbf{h}}_k$ experiences more channel hardening if

$$\frac{\mathbb{V}\left\{\|\bar{\mathbf{h}}_k\|^2\right\}}{\mathbb{E}\left\{\|\bar{\mathbf{h}}_k\|^2\right\}^2} \to 0, \text{as } M \to \infty, \tag{3}$$

where the variance and expectation is taken over the frequency and time dimensions for a given position k. This means that as the number of antennas increases, the variation of channel gain decreases. Here, the standard deviation is considered, as is also done in [15]. This means that, for a subset of M base station antennas and each position k, the instantaneous channel gain, as dependent on time and frequency, is defined as

$$\overline{G}_k(n,f) = \frac{1}{M}\sum_{m=1}^{M}\left|\bar{h}_{k,m}(n,f)\right|^2, \tag{4}$$

resulting in an average channel gain for each position of

$$\mu_k = \frac{1}{NF}\sum_{n=1}^{N}\sum_{f=1}^{F}\overline{G}_k(n,f) = 1, \tag{5}$$

which no longer depends on the number of antennas at the base station as we averaged with respect to all antennas M and will be equal to 1 due to the normalization. Note, a distinction is made between the channel gain and the array gain. The channel gain is the squared absolute value of the channel coefficient. In contrast, an array gain is here the sum of the channel gains of each antenna relative to the channel gain of a single antenna case. The array gain implies an additional gain of having multiple antennas, i.e., an array.

Finally, the standard deviation of the channel gain at a given position k can be computed as

$$\sigma_k = \sqrt{\frac{1}{NF}\sum_{n=1}^{N}\sum_{f=1}^{F}\left|\overline{G}_k(n,f) - \mu_k\right|^2}, \tag{6}$$

which is used to quantify the channel hardening by taking the difference between the complete set of base station antennas and one base station antenna.

Correlation coefficient: To compare the channel correlation between different channel pairs, the correlation coefficient[2] is studied. It is defined between two channel

2. To be complete, the correlation coefficient here defined is not the same as the correlation coefficient usually used in statistics.

vectors $\mathbf{h}_i$ and $\mathbf{h}_j$ as

$$\delta_{i,j}(n,f) = \frac{\left|\bar{\mathbf{h}}_i(n,f)^H \cdot \bar{\mathbf{h}}_j(n,f)\right|}{\left\|\bar{\mathbf{h}}_i(n,f)\right\|\left\|\bar{\mathbf{h}}_j(n,f)\right\|}, \tag{7}$$

where the channels are normalized according to (2). The correlation coefficient is estimated by picking two random measurement locations (i and j). From these locations, we select one random snapshot (n) and frequency point (f) and use these channel vectors to compute the correlation coefficient. The correlation coefficient depicts the antenna-averaged channel correlation between two channel instances. In case of uncorrelated channels, the coefficient is zero, while the coefficient is one for channels which are parallel, i.e., equal up to a scaling factor.

Channel correlation: The channel correlation matrix per position is obtained as the mean over N snapshots of the user channel and its transposed channel conjugate for the same number of samples.

$$\mathbf{R} = \frac{1}{NF}\sum_{n=1}^{N}\sum_{f=1}^{F}\bar{\mathbf{h}}(n,f)\bar{\mathbf{h}}^H(n,f), \tag{8}$$

where $\mathbf{R} \in \mathbb{C}^{M\times M}$. It expresses the correlation between the channels observed by each antenna.

The condition number: The joint orthogonality of multiple positions, or channels, is investigated by using the condition number [26], [27]. It is defined as

$$\kappa_{K,M}(n,f) = \frac{\lambda_{\max}\left(\bar{\mathbf{H}}(n,f)^H\bar{\mathbf{H}}(n,f)\right)}{\lambda_{\min}\left(\bar{\mathbf{H}}(n,f)^H\bar{\mathbf{H}}(n,f)\right)}, \tag{9}$$

with $\kappa_{K,M} \in [1,\infty)$, for M antennas and K users. The channel matrix $\bar{\mathbf{H}}(n,f)$ consists of the normalized channel instances of K positions $[\bar{\mathbf{h}}_1(n,f)\ldots\bar{\mathbf{h}}_K(n,f)] \in \mathbb{C}^{M\times K}$. A high condition number means that at least one pair of channels is strongly correlated. When all channels are pairwise orthogonal, the condition number becomes one. The inverse condition number is chosen as a metric to be able to express the orthogonality in a finite range, i.e., $\kappa_{K,M}^{-1} \in [0,1]$.

Chordal distance: The chordal distance measures the orthogonality between two eigenspaces, represented as the p-dominant eigenvectors. By definition [28], the chordal distance between two matrices $\mathbf{U}_i$ and $\mathbf{U}_j$ is given by

$$d_c(\mathbf{U}_i,\mathbf{U}_j) = \left\|\mathbf{U}_i\mathbf{U}_i^H - \mathbf{U}_j\mathbf{U}_j^H\right\|_F^2, \tag{10}$$

where $\mathbf{U}_i \in \mathbb{C}^{M\times p}$ and $\mathbf{U}_j \in \mathbb{C}^{M\times p}$ are the unitary matrices that span over the number of antennas M and p-dominant eigendirections. The unitary matrices are obtained in the eigenvalue decomposition from the Hermitian matrix $\mathbf{R}$ as follows: $\mathbf{R} = \mathbf{U}\mathbf{D}\mathbf{U}^H$. Note that in order to estimate the chordal distance it is important to obtain the p-dominant eigendirections in advance.

(a) 32-element ULA

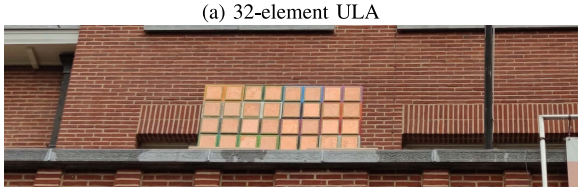

(b) 4 × 8 URA

FIGURE 1. Antenna array configurations.

III. MEASUREMENT SETUP AND SCENARIO

The 5G massive MIMO testbed at KU Leuven[3] based on National Instruments equipment was used during these experiments. The testbed runs the LabVIEW Communications MIMO Application. This application was designed for LTE-TDD based transmission. Therefore, the LabView application had to be adapted to conform to the regulations of [29]. To be precise, the occupied bandwidth, the transmit power and duty cycle of the framework had to be altered. This is elaborated on in [24]. Table 1 summarizes the measurement setup.

The base station is, as mentioned before, equipped with 32 vertically polarized patch antennas. Two array configurations were used, a 4-by-8 URA (Fig. 1(b)) and a 32-element ULA (Fig. 1(a)). The patch antenna was designed to operate in the 868 MHz band. In theoretical massive MIMO papers a 32-element array may be considered relatively small, yet in absolute terms at this operation frequency the array is definitely quite large, i.e., 5.5 m for a 32-element ULA at 868 MHz or with a wavelength of 34.5 cm. The array consists of two-element holders. These holders facilitate the design of different array topologies. While in this measurement we use a rectangular and a linear uniformal array, cylindrical and distributed arrays can be easily constructed with this design. At the node side, a single dipole antenna is used (Fig. 2).

The measurements were conducted in front of the Department of Electrical Engineering (ESAT) building in Heverlee, Belgium. The measurement environment can be seen in Fig. 3. The base station was placed on the balcony at the first floor of the building at a height of 7 m.

During the experimental campaign, we collected the channels on all 32 antennas for static and continuous measurements. Between each static measurement position we moved the transmit antenna (node) 10 meters according to the paths shown in Fig. 3. The paths were chosen in order to have positions perpendicular and parallel to the base station,

3. https://www.esat.kuleuven.be/telemic/research/NetworkedSystems/infrastructure/massive-mimo-5g

FIGURE 2. Transmit node with a single dipole antenna.

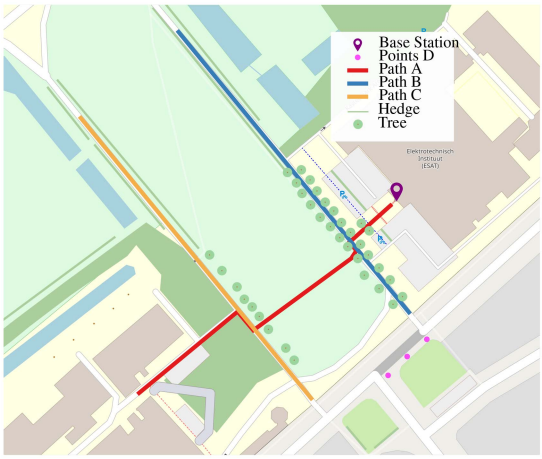

FIGURE 3. Overview of rural measurement area. All paths have a length of approximately 140 m.

as well as having NLoS and LoS positions. As the measurements were done in summer, the presence of foliage on the trees has a non-negligible effect on the collected channels. Both the measurement data[4] and the processing scripts[5] are available in open-source.

When comparing LoS and NLoS scenarios, we use two static points per case. The locations of the measurement points are shown in Fig. 4 and further used in Section IV to study the effect of LoS and NLoS scenarios.

IV. EVALUATION

We here evaluate different performance metrics, grouped based on their impact on crucial aspects for IoT communication. Section IV-A explores the benefits of massive MIMO regarding the reliability, coverage and energy efficiency of the IoT nodes. The ability to serve multiple nodes and a first look on how to schedule them is studied in Sections IV-B and IV-C.

4. dramco.be/massive-mimo/measurement-selector/#Sub-GHz
5. github.com/GillesC/MARRMOT

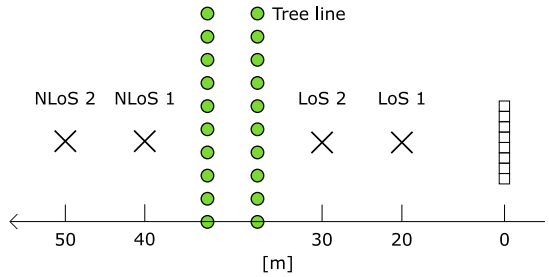

FIGURE 4. Points considered to be LoS and NLoS including distances (in m) with respect to the base station.

When investigating the impact of the number of base station antennas, we selected M_s subsequent array elements according to their numbering. In the case of a ULA this always results in a ULA of M_s antenna elements, this in contrast to selecting random antenna elements. The same reasoning does not always hold for the URA configuration. An example where this does not hold is shown in Fig. 5. Consequently, the results of the URA configuration, with respect to the number of antennas, needs to be carefully interpreted. To be able to capture small-scale fading, while still have a negligible effect of the large-scale fading, we divided the continuous measurements in paths with a length of approximately $25\,\lambda$.

A. INCREASED ENERGY EFFICIENCY, COVERAGE AND RELIABILITY

The reliability, coverage and energy efficiency improvement are assessed by means of the channel gain diversity, combining gain and channel hardening effect. The combining gain allows reducing the transmit power of the nodes thanks to the increased gain when combining the many base station antennas. Equivalently, the coverage can be extended by the achieved combined gain. Furthermore, when a channel offers channel hardening, the variance of the channel gain decreases as the number of antennas increases, hence providing a more reliable channel. As a result, the fading margin at the IoT node can also be reduced. As the channel becomes more deterministic, the probability of packet losses decreases, and thereby the number of required retransmissions is reduced.

Channel Gain Diversity over the Array: In [16], it was observed that antenna arrays with a large aperture experience antenna-dependent large-scale fading. In this work, we have observed similar behavior even with a low number of antennas. Notably, the physical aperture of the array is larger for 868 MHz than 2.6 GHz as in [16]. The un-normalized average channel gain, summed over frequency and per base station antenna, is depicted in Fig. 6 for the two array configurations and a LoS and NLoS scenario respectively. By averaging the channel gain over time for each antenna element, we take away the small-scale fading present on each antenna. Fig. 6 shows that the large-scale fading can not be considered constant over the antennas as is frequently assumed in theoretical work [12]. Depending on the position of the antenna in the array, it can be shadowed or

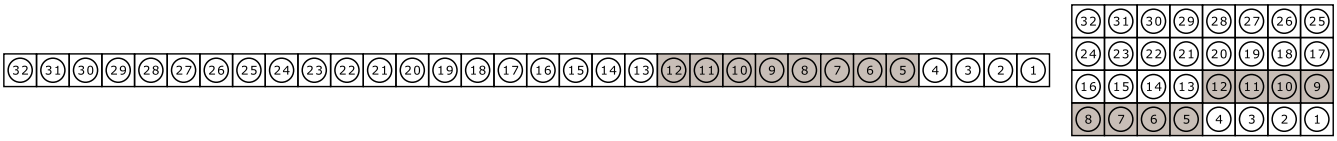

FIGURE 5. Antenna numbering with 8 randomly selected subsequent antenna elements (highlighted).

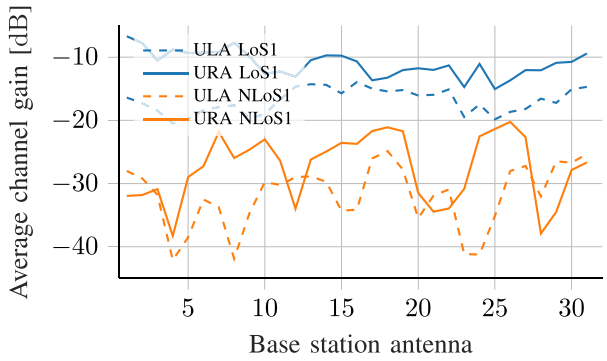

FIGURE 6. The average (over time) channel gain per antenna element demonstrates the presence of varying large-scale fading over the antennas. The antenna numbering is according to Fig. 5.

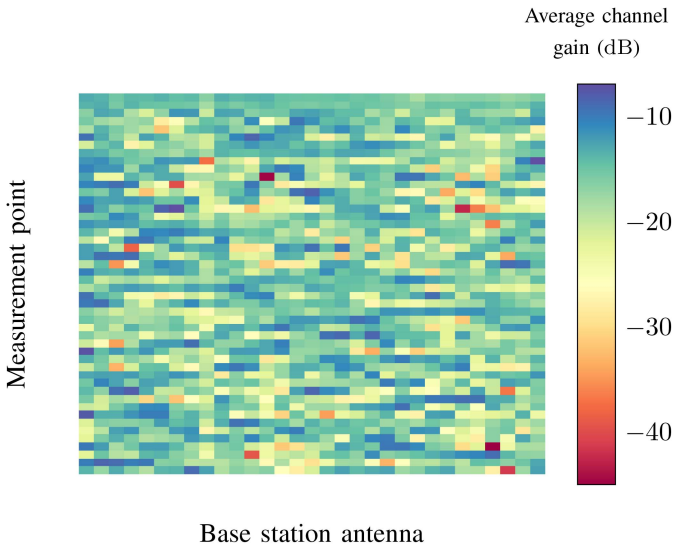

FIGURE 7. Average channel gain per base station antenna (ULA). Each row depicts the average channel gain per measurement point for each antenna element.

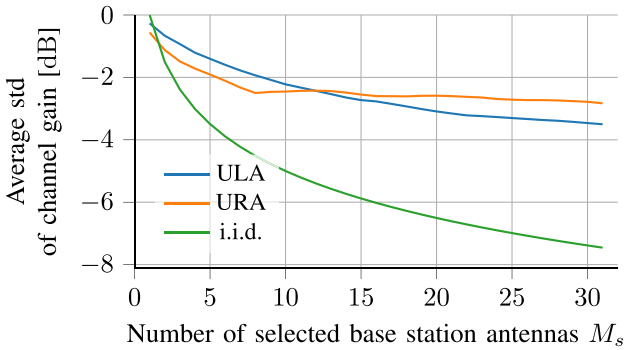

FIGURE 8. Average standard deviation of channel gain (6) when increasing the number of antennas for the ULA and URA.

see different multi-path components; this naturally becomes even more noticeable in the NLoS scenario for both array configurations. The average observed difference between the maximum and minimum channel coefficients between two antennas during one measurement is 15.4 dB and 13.2 dB for the ULA and URA, respectively. Depending on the location of the node and how the multi-path components travel in the environment, the antennas at the base station will hence not contribute equally to the overall received signal. Fig. 7 illustrates this by showing the average channel gain for all base station antennas and all measured points. The considerable differences demonstrate that spatial diversity can significantly improve the link reliability. It can also be noted that at some points, a specific antenna can be in a fading dip while being one of the strongest antennas at other points.

Channel Hardening: When increasing the number of antennas, the channel hardening effect appears. For a Rayleigh fading channel, the channel hardening becomes $10\log_{10}(\sqrt{M})$ when using the standard deviation for comparison as in (6). The channel hardening is here measured as the difference of the standard deviation of the channel gain when going from 1 to M antennas, i.e., 7.5 dB with 31 antennas. A comparison between i.i.d. Rayleigh fading and the measured channel with the ULA and the URA is shown in Fig. 8. Here, the average standard deviation of channel gain of a time window of size 600 for an increasing number of antennas is depicted, extracted from the continuous measurements along path B and C in Fig. 3. The antennas are chosen in the order that is outlined in Fig. 5.

In Fig. 8, a clear channel hardening effect can be seen as the standard deviation of channel gain decreases when the number of base station antennas increases. In the beginning the URA has a lower standard deviation than the ULA until eight antennas where it saturates and is then bypassed by the ULA. For the ULA the average channel hardening is 3.2 dB and for the URA it is 2.3 dB. The reason for more channel hardening with the ULA is most likely due to better possibilities of exploiting the spatial diversity while adding more rows to the URA does not contribute as much. The channel hardening effect allows to reduce the fading margins and therefore the overall transmit power as well.

B. SERVING MULTIPLE NODES

The channel orthogonality is assessed by means of the correlation coefficient and the inverse condition number of channels captured at different measurement locations. The

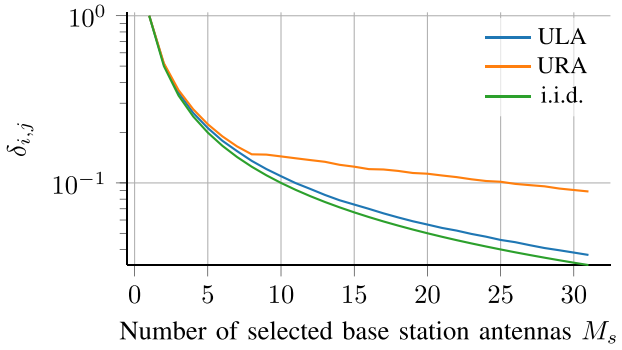

FIGURE 9. Average node correlation $\delta_{i,j}$ in (7) between the channel vectors of two random node positions, as a function of the number of BS antennas. Expressed in dB to better illustrate the difference between the graphs.

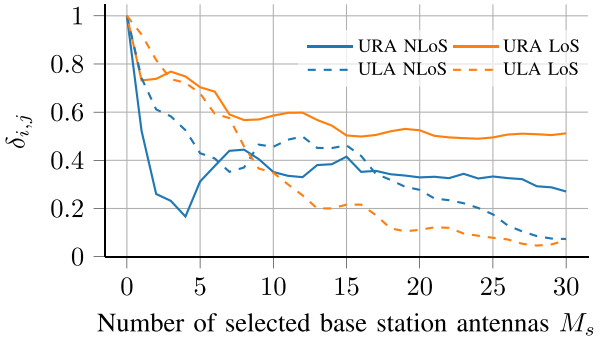

FIGURE 10. Correlation coefficient $\delta_{i,j}$ between the two LoS and NLoS users.

former describes the orthogonality of two nodes, while the latter shows the joint channel orthogonality of multiple nodes. Both metrics are evaluated with respect to the number of base station antennas. We consider on average 300 locations per antenna configuration. The actual static locations were extended with virtual locations by splitting the continuous measurements in virtual locations, each with 100 channel instances, equivalent to capturing 1 second.

Correlation Coefficient: The correlation coefficient relates to the concept of favorable propagation, which also quantifies the ability to separate channels. When there is favorable propagation [28], the channel vectors are pair-wise orthogonal such that $\frac{1}{M}\mathbf{h}_i{}^H\mathbf{h}_j \to 0$ as $M \to \infty$ for two positions i and j.

Fig. 9 depicts the correlation between two channel instances from two random locations as a function of the number of base station antennas. The result was obtained by calculating the correlation coefficient – as defined in (7) – 100 000 times per antenna configuration and for different numbers of consecutive antennas. For i.i.d. Rayleigh fading the average correlation coefficient becomes $1/M$ [28]. Fig. 9 shows the same trend for the ULA, URA and i.i.d. Rayleigh fading for the first eight antennas. After eight antennas the decrease of the correlation flattens for the URA, demonstrating that adding a second row does not contribute as much to the decorrelation of the channels. This effect is much smaller in the ULA case, illustrating that increasing the size of the ULA increases the spatial diversity, as was also observed when studying the channel hardening.

The correlation between the channels for a LoS and NLoS case is shown in Fig. 10. The general trend shows that the ULA configuration captures channels which are less correlated than the URA configuration. Moreover, when deploying close to 32 antennas, the correlation coefficient for both NLoS and LoS becomes equal. Hence, even in LoS, increasing the number of antenna elements in a ULA configuration contributes to the decorrelation of the channel coefficients such that nodes could be separated. However, for the URA, as expected this is trickier in LoS and the decorrelation of users is much more prominent in the NLoS scenario.

Orthogonality of Multiple Nodes: The orthogonality of multiple IoT nodes is assessed by examining the condition number [27] or the distance from favorable propagation [13]. The normalization and the channel instance selection procedure are equivalent to that explained in Section IV-B.

A large condition number implies strongly correlated channels, while a condition number of one indicates pairwise orthogonal channels. The inverse condition number is chosen as a metric to be able to express the orthogonality in a finite range, i.e., $\kappa^{-1} \in [0, 1]$. The inverse condition number for two, five and ten users as a function of the number of base station antennas is shown in Fig. 11(a). The users are randomly selected as discussed in Section IV-B. Logically $\kappa^{-1}_{K,M}$ equals zero as long as K is larger than M.

We see that the $\kappa^{-1}_{K,M}$ of the ULA follows closely the ideal i.i.d. Rayleigh fading case and tends to move closer to this curve as the number of base station antennas increases; for the URA case, the distance from i.i.d Rayleigh fading is larger.

The empirical cumulative distribution function (CDF) is used to further elaborate on the impact of K and M in Fig. 11(b). There exist some strongly correlated channels, as is illustrated by the spread of $\kappa^{-1}_{K,M}$ over the entire range $[0, 1]$. This is also noticeable in the CDF of the correlation coefficient (Fig. 11(b)) as both ULA and URA show some correlation coefficients close to one. While there are not many strongly correlated signals, it still demonstrates the importance of adequate user grouping and scheduling.

C. SCHEDULING IOT NODES

Dominant Eigen directions: As demonstrated with previous metrics, we cannot assume i.i.d. Rayleigh fading channels but expect that signals, coming from the IoT nodes, have distinct directions. In other words, we expect that in this setting, nodes have dominant directions which do not change drastically over time. These dominant directions and their significance are studied by their eigendirections and could be used to schedule nodes.

The distribution of weak and strong eigendirections can be extracted from the channel correlation matrix $\mathbf{R}$ as defined in (8) [28]. The correlation matrix is obtained from the continuous channel collection along path B and C for a

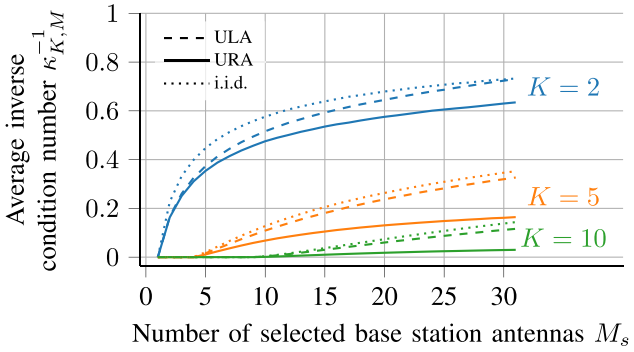

(a) The average inverse condition number $\kappa_{K,M}^{-1}$ for K IoT nodes and 32 antennas.

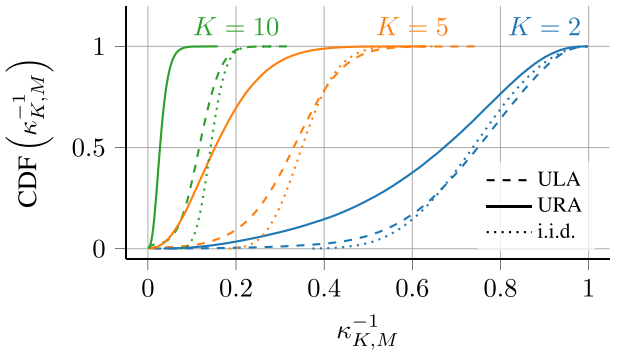

(b) CDF of the inverse condition number $\kappa_{K,M}^{-1}$ for K IoT nodes and 32 antennas.

FIGURE 11. The average and CDF of the inverse condition number $\kappa_{K,M}^{-1}$ for K IoT nodes and 32 antenna.

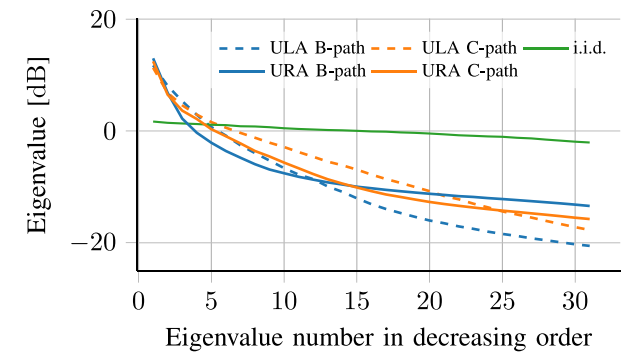

FIGURE 12. Eigenvalues ordered in descending order for different antenna topologies and different positions.

time window of size 600 samples, corresponding to approximately 25λ. A diagonal matrix **D** containing the eigenvalues is obtained through the eigenvalue decomposition of the correlation matrix. The eigenvalues are sorted in descending order. The higher the values of the first eigenvalues, the more energy is confined in a few eigendirections. Fig. 12 depicts the eigenvalues tr(**D**) of the channels for path C and B in Fig. 4. Most of the energy – between 68% and 85% – is carried by three eigendirections, regardless of the antenna array and node position. As we have a finite number of measured channel instances, the i.i.d. Rayleigh fading channel is also simulated with the same number of snapshots.

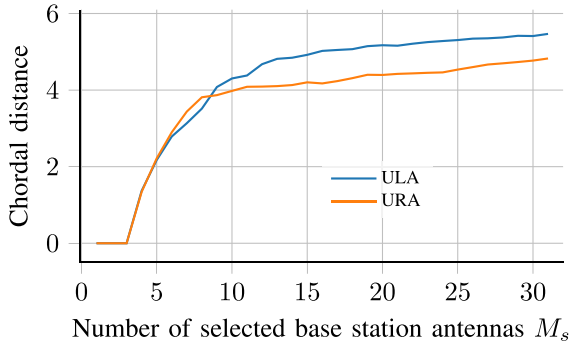

FIGURE 13. Chordal distance of 3-dominant eigenspaces between path B and C for the ULA and URA configuration.

Fig. 12 shows that the eigenvalues are distributed around 0 dB, whereas asymptotically all eigenvalues will be equal. Fig. 12 further reveals that the experimentally captured data are close to the asymptotic case. We can conclude that for both configurations and both paths, dominant directions are present. The latter is in contrast to the simulated i.i.d. case. The ULA and URA show similar trends on both paths.

The difference between the three dominant eigendirections is measured by computing the chordal distance, defined in (10). The chordal distance is used in [30], [31] to reduce the complexity when selecting users to be scheduled together, while still performing similar to full-CSI selection algorithms. Fig. 13 presents the average chordal distance between the 3-dominant eigenspaces of paths B and C. This figure shows the degree of orthogonality of the eigenspaces between the aforementioned configurations. As expected, the difference between the eigenspaces increases when the number of antennas increases. The ULA increases the distance between the three eigenspace more rapidly by increasing the number of base station antennas, while with the URA it stagnates after 8 antennas.

V. OUTLOOK AND CONCLUSION

In this paper, we have studied the opportunities of massive MIMO technology to upgrade LPWANs operating in the unlicensed sub-GHz band for future IoT applications. We have evaluated several relevant performance metrics, based on measurement data gathered through an experimental campaign; this data is now available open-source.

Based on the measurements, we observed the favorable effects expected in massive MIMO as of 32 antennas. The experimental campaign covered both LoS and NLoS scenarios, and ULA and URA antenna array configurations were deployed. Our assessment confirms that both array gain and channel hardening are considerable, while not always present in all scenarios [32], [33]. Hence, when combining the many antennas properly, the power consumption of the nodes can be reduced drastically and the link reliability can be increased. For example, for the case of a 32-antenna gateway, this could specifically allow the battery-powered IoT devices to reduce their transmit power by M – or $10\log_{10}(M)$ dB.

Alternatively, the additional combining gain could be used to extend the coverage. Furthermore, the fading margins can be lowered due to the channel hardening effect. This effect also ensures that fewer retransmissions are required, which are shown in [34] to account for considerable energy consumption in current LPWAN technologies.

We performed an analysis of joint orthogonality of channels for different node positions. It shows that the relatively large array does receive quite different responses from these positions, opening the opportunity for spatial multiplexing of nodes. When comparing the URA and ULA, it is noticeable that whereas the received gains of both are similar, the channel correlation between different positions are quite different. This indicates that the average channel power per antenna is similar for both configurations, but the linear array also ensures a more diverse set of paths is received. The latter facilitates better decorrelation of nodes and is hence better suited for serving many nodes. Noteworthy is that even with users perpendicular to the array, the ULA still performs better than the URA. The ULA also outperforms the URA when users have the same azimuth angle with respect to the base station, as shown in Fig. 10.

The measured channels show the presence of a few dominant eigendirections that could be used for scheduling users. It also demonstrates that i.i.d. Rayleigh fading does not hold in the considered typical outdoor LoS and NLoS scenarios. New models need to be designed to include sub-GHz massive MIMO propagation. These models can then be used to design new low-power IoT protocols, to provide a massive amount of devices energy-efficient access.

ACKNOWLEDGMENT

The authors would like to thank Vladimir Volski for designing the path antenna, Sofie Pollin for her help with the Massive MIMO testbed configuration, François Rottenberg for the fruitful discussions and their colleagues of Dramco for assisting them during the experiments.

REFERENCES

[1] G. Callebaut and L. Van der Perre, "Characterization of LoRa point-to-point path loss: Measurement campaigns and modeling considering censored data," *IEEE Internet Things J.*, vol. 7, no. 3, pp. 1910–1918, Mar. 2020.

[2] M. Xhonneux, J. Tapparel, O. Afisiadis, A. Balatsoukas-Stimming, and A. Burg, "A maximum-likelihood-based multi-user LoRa receiver implemented in GNU Radio," in *Proc. 54th Asilomar Conf. Signals Syst. Comput.*, Nov. 2020, pp. 1106–1111.

[3] M. N. Mahfoudi, G. Sivadoss, O. B. Korachi, T. Turletti, and W. Dabbous, "Joint range extension and localization for low-power wide-area network," *Internet Technol. Lett.*, vol. 2, no. 5, p. e120, 2019. [Online]. Available: https://onlinelibrary.wiley.com/doi/abs/10.1002/itl2.120

[4] A. Dongare *et al.*, "Charm: Exploiting geographical diversity through coherent combining in low-power wide-area networks," in *Proc. 17th ACM/IEEE Int. Conf. Inf. Process. Sens. Netw. (IPSN)*, 2018, pp. 60–71.

[5] A. Hoeller, R. D. Souza, O. L. A. López, H. Alves, M. de Noronha Neto, and G. Brante, "Analysis and performance optimization of LoRa networks with time and antenna diversity," *IEEE Access*, vol. 6, pp. 32820–32829, 2018.

[6] E. Björnson, E. de Carvalho, J. H. Sorensen, E. G. Larsson, and P. Popovski, "A random access protocol for pilot allocation in crowded massive MIMO Systems," *IEEE Trans. Wireless Commun.*, vol. 16, no. 4, pp. 2220–2234, Apr. 2017.

[7] A.-S. Bana *et al.*, "Massive MIMO for Internet of Things (IoT) connectivity," *Phys. Commun.*, vol. 37, Dec. 2019, Art. no. 100859, [Online]. Available: http://www.sciencedirect.com/science/article/pii/S1874490719303891

[8] B. M. Lee and H. Yang, "Massive MIMO for Industrial Internet of Things in cyber-physical systems," *IEEE Trans. Ind. Informat.*, vol. 14, no. 6, pp. 2641–2652, Jun. 2018.

[9] L. Liu and W. Yu, "Massive connectivity with massive MIMO—Part I: Device activity detection and channel estimation," *IEEE Trans. Signal Process.*, vol. 66, no. 11, pp. 2933–2946, Jun. 2018.

[10] N. Saxena, A. Roy, B. J. R. Sahu, and H. Kim, "Efficient IoT gateway over 5G wireless: A new design with prototype and implementation results," *IEEE Commun. Mag.*, vol. 55, no. 2, pp. 97–105, Feb. 2017.

[11] B. M. Lee, "Improved energy efficiency of massive MIMO-OFDM in battery-limited IoT networks," *IEEE Access*, vol. 6, pp. 38147–38160, 2018.

[12] K. Senel and E. G. Larsson, "Grant-free massive MTC-enabled massive MIMO: A compressive sensing approach," *IEEE Trans. Commun.*, vol. 66, no. 12, pp. 6164–6175, Dec. 2018.

[13] H. Q. Ngo, E. G. Larsson, and T. L. Marzetta, "Aspects of favorable propagation in massive MIMO," in *Proc. 22nd Eur. Signal Process. Conf. (EUSIPCO)*, 2014, pp. 76–80.

[14] S. Gunnarsson, L. Van der Perre, and F. Tufvesson, *Massive MIMO Channels*, Amer. Cancer Soc., Atlanta, GA, USA, 2020. [Online]. Available: https://onlinelibrary.wiley.com/doi/abs/10.1002/9781119471509.w5GRef040

[15] S. Willhammar, J. Flordelis, L. Van der Perre, and F. Tufvesson, "Channel hardening in massive MIMO: Model parameters and experi-mental assessment," *IEEE Open J. Commun. Soc.*, vol. 1, pp. 501–512, 2020.

[16] X. Gao, O. Edfors, F. Rusek, and F. Tufvesson, "Massive MIMO performance evaluation based on measured propagation data," *IEEE Trans. Wireless Commun.*, vol. 14, no. 7, pp. 3899–3911, Jul. 2015.

[17] X. Gao, O. Edfors, F. Tufvesson, and E. G. Larsson, "Massive MIMO in real propagation environments: Do all antennas contribute equally?" *IEEE Trans. Commun.*, vol. 63, no. 11, pp. 3917–3928, Nov. 2015.

[18] M. Arnold and S. T. Brink, "Properties of measured massive MIMO channels using different antenna geometries," in *Proc. 23rd Int. ITG Workshop Smart Antennas*, 2019, pp. 1–5.

[19] M. Tran, O. Gustafsson, P. Källström, K. Senel, and E. G. Larsson, "An architecture for grant-free massive MIMO MTC based on compressive sensing," in *Proc. 53rd Asilomar Conf. Signals Syst. Comput.*, 2019, pp. 901–905.

[20] Y. Beyene, C. Boyd, K. Ruttik, C. Bockelmann, O. Tirkkonen, and R. Jäntti, "Compressive sensing for MTC in new LTE uplink multi-user random access channel," in *Proc. AFRICON*, 2015, pp. 1–5.

[21] F. A. P. de Figueiredo, F. A. Cardoso, J. P. Miranda, I. Moerman, C. F. Dias, and G. Fraidenraich, "Large-scale antenna systems and massive machine type communications," *Int. J. Wireless Inf. Netw.*, vol. 27, pp. 317–339, Jun. 2020.

[22] X. Cai, G. Zhang, C. Zhang, W. Fan, J. Li, and G. F. Pedersen, "Dynamic channel modeling for indoor millimeter-wave propagation channels based on measurements," *IEEE Trans. Commun.*, vol. 68, no. 9, pp. 5878–5891, Sep. 2020.

[23] A. Garcia-Rodriguez, G. Geraci, L. G. Giordano, A. Bonfante, M. Ding, and D. López-Pérez, "Massive MIMO unlicensed: A new approach to dynamic spectrum access," *IEEE Commun. Mag.*, vol. 56, no. 6, pp. 186–192, Jun. 2018.

[24] G. Callebaut *et al.*, "Massive MIMO goes Sub-GHz: Implementation and experimental exploration for LPWANs," in *Proc. 54th Asilomar Conf. Signals Syst. Comput.*, 2020, pp. 1101–1105.

[25] H. Q. Ngo and E. G. Larsson, "No downlink pilots are needed in TDD massive MIMO," *IEEE Trans Wireless Commun*, vol. 16, no. 5, pp. 2921–2935, May 2017.

[26] J. Maurer, G. Matz, and D. Seethaler, "Low-complexity and full-diversity MIMO detection based on condition number thresholding," in *Proc. IEEE Int. Conf. Acoust. Speech Signal Process.*, vol. 3, 2007, pp. 61–64.

[27] J. Hoydis, C. Hoek, T. Wild, and S. Ten Brink, "Channel measurements for large antenna arrays," in *Proc. Int. Symp. Wireless Commun. Syst. (ISWCS)*, 2012, pp. 811–815.
[28] E. Björnson, J. Hoydis, and L. Sanguinetti, "Massive MIMO networks: Spectral, energy, and hardware efficiency," *Found. Trends Signal Process.*, vol. 11, nos. 3–4, pp. 154–655, 2017. [Online]. Available: http://dx.doi.org/10.1561/2000000093
[29] E. CEPT, *ERC Recommendation 70-03, Relating to the Use of Short Range Devices (SRD)*, Electron. Commun. Committee, 2017.
[30] B. Zhou, B. Bai, Y. Li, D. Gu, and Y. Luo, "Chordal distance-based user selection algorithm for the multiuser MIMO downlink with perfect or partial CSIT," in *Proc. IEEE Int. Conf. Adv. Inf. Netw. Appl.*, 2011, pp. 77–82.
[31] M. Taniguchi *et al.*, "Indoor experiment of multi-user MIMO user selection algorithm based on chordal distance," in *Proc. IEEE Global Commun. Conf. (GLOBECOM)*, 2013, pp. 3959–3964.
[32] C. Qin, Y. Miao, Y. Gao, J. Chen, J. Zhang, and A. Glazunov, "Simulation-based investigation on spatial channel hardening of massive MIMO in different indoor scenarios and with different array topologies," in *Proc. XXXIIIrd Gen. Assembly Sci. Symp. Int. Union Radio Sci.*, 2020, pp. 1–4.
[33] S. Li, P. J. Smith, P. A. Dmochowski, H. Tataria, M. Matthaiou, and J. Yin, "Massive MIMO asymptotics for ray-based propagation channels," *IEEE Trans. Wireless Commun.*, vol. 19, no. 6, pp. 3977–3991, Jun. 2020.
[34] G. Callebaut, G. Ottoy, and L. Van der Perre, "Cross-layer framework and optimization for efficient use of the energy budget of IoT nodes," in *Proc. IEEE Wireless Commun. Netw. Conf. (WCNC)*, 2019, pp. 1–6.

GILLES CALLEBAUT received the M.Sc. degree *(summa cum laude)* in engineering technology from KU Leuven (Ghent Campus), Belgium, in 2016, where he is currently pursuing the Ph.D. degree in massive MIMO for low power machine type communication. He initiated the tutorial "Low Power Wireless Technologies for Connecting Embedded Sensors in the IoT: A Journey From Fundamentals to Hands-On." He is currently a Member of Dramco, a Research Group which is focused on wireless and mobile communication systems. He received the Laureate Award.

SARA WILLHAMMAR (Member, IEEE) received the M.Sc. degree in electrical engineering from Lund University in 2017. She is currently pursuing the double Ph.D. degree in collaboration with the Department of Electrical and Information Technology, Lund University, Sweden, and the Department of Electrical Engineering, KU Leuven, Belgium. Her main research interests are channel characterization and modeling to improve reliability and efficiency in massive MIMO systems.

ANDREA P. GUEVARA received the B.Sc. degree in electronics and telecommunications from the University of Cuenca, Ecuador, in 2013, and the M.Sc. degree in telecommunications by Research in 2015 and the prize for the best academic performance on an M.Sc. by research programme from the Faculty of Natural and Mathematical Sciences, King's College London, U.K. She is currently pursuing the Ph.D. degree with KU Leuven. Her main interests are massive MIMO, infrastructure sharing, beamforming, and power leakage.

ANDERS J. JOHANSSON (Member, IEEE) received the M.S., Lic.Eng., and Ph.D. degrees in electrical engineering from Lund University, Lund, Sweden, in 1993, 2000, and 2004, respectively. From 1994 to 1997, he was with Ericsson Mobile Communications AB, developing transceivers and antennas for mobile phones. Since 2005, he has been an Associate Professor with the Department of Electrical and Information Technology, Lund University. His research interests include antennas, wave propagation, and telemetric devices for medical implants, as well as antenna systems and propagation modeling for MIMO systems.

LIESBET VAN DER PERRE (Member, IEEE) is a Professor with the Department of Electrical Engineering, KU Leuven, Leuven, Belgium, and a Guest Professor with the Electrical and Information Technology Department, Lund University, Sweden. She was with the Nano-Electronics Research Institute imec, Belgium, from 1997 to 2015. She was appointed as an Honorary Doctor with Lund University, Sweden, in 2015. Her main research interests are in wireless communication, with a focus on physical layer and energy efficiency in both broadband communication and IoT.

FREDRIK TUFVESSON (Fellow, IEEE) received the Ph.D. degree from Lund University, Lund, Sweden, in 2000. After two years at a startup company, he joined the Department of Electrical and Information Technology, Lund University, where he is currently Professor of Radio Systems. His main research interests include the interplay between the radio channel and the rest of the communication system, with various applications in 5G systems. He recently received the Neal Shepherd Memorial Award for the Best Propagation Paper in the IEEE TRANSACTIONS ON VEHICULAR TECHNOLOGY and the IEEE COMMUNICATIONS SOCIETY Best Tutorial Paper Award.